Uniform Lithium Nucleation Guided by Atomically Dispersed Lithiophilic CoN$_x$ Sites for Safe Lithium Metal Batteries

*He Liu, Xiang Chen, Xin-Bing Cheng, Bo-Quan Li, Rui Zhang, Bin Wang, Xiao Chen, and Qiang Zhang**

The mossy lithium dendrite growth during repeated lithium plating/stripping induces low Coulombic efficiency, poor lifespan, and safety concerns of working lithium metal batteries. Herein, atomically dispersed CoN$_x$-doped graphene is exploited as a host to accommodate dendrite-free lithium deposits. The coordination between Co and N in the conductive matrix can effectively regulate the local electronic structure, and thereby enhance the adsorption of lithium ions and promote the following nucleation process. Meanwhile, the doped N facilitates high dispersion of Co atoms into graphene through the Co—N coordination bond. The strong lithiophilicity provided by N coordinated with Co promises a uniform lithium nucleation behavior, further contributing to the smooth lithium deposition morphology. These characteristics afford a superhigh Coulombic efficiency of 99.2% at 2.0 mA cm^{-2} (≈400 cycles) and 5.0 mA cm^{-2} (350 cycles), and 98.2% at 10.0 mA cm^{-2} (200 cycles) with a capacity of 2.0 mAh cm^{-2}. LiFePO$_4$|CoNC–Li full cells deliver a long lifespan of 340 cycles at 1.0 C (240 cycles for routine cells). This offers fresh insights into effectively regulating the lithiophilic chemistry of lithium metal host toward uniform nucleation and growth of lithium deposits in working high-energy-density batteries.

The continuously growing energy demands for next-generation storage devices, such as electric vehicles and smart grid storage, result in a never ending thirst for high-capacity electrode materials beyond those in lithium-ion batteries (LIBs).[1,2] In this regard, lithium (Li) metal holds great promises for revolutionizing the current rechargeable battery technologies due to its ultrahigh theoretical specific capacity (3860 mAh g^{-1}) and the lowest redox potential (–3.040 V vs the standard hydrogen electrode).[3–6] Li metal batteries (LMBs) can theoretically offer 5 to 10 times increased overall energy density compared to current LIBs, which is strongly desired for the next-generation energy storage applications.[7–11] Nevertheless, Li metal anode suffers from serious Li dendrite issues induced by the uneven Li nucleation/deposition and unstable solid electrolyte interphase (SEI) films due to the highly active nature of Li metal. This leads to serious safety concerns, poor cycling efficiency, and a short lifespan of LMBs.[12–16]

Remarkable achievements have been achieved to address these issues involved in Li metal anodes, including exploiting electrolyte additives to construct stable SEI films,[17–20] designing high-modulus solid/composite electrolytes to impede dendrite penetration,[21–27] and engineering stable artificial interfacial layers to inhibit dendrite growth.[28–32] However, the relatively infinite volume change induced by the hostless feature of Li plating/stripping at a high areal capacity is a formidable challenge. A host that can accommodate Li is therefore strongly considered.[33] Numerous 3D carbon-based materials have emerged as promising hosts to plate Li and relieve the volume change, reduce the local current density, as well as achieve a stable SEI film.[34–40] Nevertheless, the intrinsic poor affinity of Li metal to the surface of carbon host results in remarkable nucleation barriers, which is unfavorable for uniform Li deposition.[41–44] The initial nucleation manner primarily influences the Li deposition behavior and the final morphology.[45,46]

The introduction of heteroatoms is an emerging strategy to tailor the surface chemistry of nanocarbon materials to reduce the nucleation overpotential.[47,48] Of note is that the lithiophilic sites in the matrix need to be homogenous enough to guarantee the uniformity of nucleation sites. Otherwise, uncontrollable dendrite growth cannot be avoided. Additionally, adequate amounts of N doping can largely increase the lithiophilicity of carbon matrix, while negatively result in the destruction of structural integrity and the decrease of electrical conductivity. If the lithiophilic sites can be built with tunable lithiophilicity, the dendrite-free Li metal deposits can be therefore achieved.

In this contribution, the concept of atomically dispersed CoN$_x$-doped carbon (CoNC) is proposed to regulate

---

Dr. H. Liu, X. Chen, Dr. X.-B. Cheng, B.-Q. Li, R. Zhang, Dr. B. Wang,
Dr. X. Chen, Prof. Q. Zhang
Beijing Key Laboratory of Green Chemical Reaction
Engineering and Technology
Department of Chemical Engineering
Tsinghua University
Beijing 100084, P. R. China
E-mail: zhang-qiang@mails.tsinghua.edu.cn

The ORCID identification number(s) for the author(s) of this article can be found under https://doi.org/10.1002/smtd.201800354.

DOI: 10.1002/smtd.201800354

Li nucleation and deposition behavior in working Li metal batteries. The coordination between single Co atom and surrounding N in the carbon matrix can effectively tailor the local electronic structure, and thereby optimize the adsorption of Li ions and promote the following nucleation process. Additionally, the sparsely distributed doped N facilitates the high dispersion of Co atoms embedded into graphene through the Co—N coordination bond, resulting in atomically dispersed CoN_x sites. The hierarchical porous structure with high density and dispersion of CoN_x moieties renders a uniform Li nucleation and deposition behavior. This contributes to a remarkable electrochemical performance with an ultrahigh and stable Coulombic efficiency (CE), a low nucleation overpotential, and a small deposition polarization even at a current density as high as 10.0 mA cm^{-2}. In a full cell with $LiFePO_4$ (LFP) cathode, CoNC–Li composite anode also displays excellent cycling stability and superb rate capability.

The N heteroatoms are coordinated to Co atoms to form $Co—N_x—C$ moieties in conductive CoNC hosts. The strong Co—N interaction contributes to charge transfer from metal dopants to the carbon matrix, leading to an electronically rich environment of the neighboring C and N atoms.[49,50] The higher electronegativity of CoN_x center in CoNC matrix than N site in routine N-doped graphene renders stronger affinity to Li ions, namely higher lithiophilicity. As a result, Li prefers to nucleate on these CoN_x sites (**Figure 1**). It is theoretically revealed that the metal–N_x–C structures are more energetically feasible to form at graphitic edges.[51] Hence, it can be inferred that Co species tends to coordinate with the N dopants at defective edges or pores of graphene, facilely achieving atomic dispersion of CoN_x moieties. These atomically dispersed CoN_x guarantees highly uniform nucleation sites in the CoNC materials, which is of great significance for achieving a desired plating/stripping process in the subsequent cycles. Consequently, the doped Co and N species synergistically promote the Li nucleation and deposition behavior in Li metal anodes.

The CoNC materials were obtained via the direct carbonization of a mixture of carbon sources, nitrogen sources, cobalt sources, and in situ generated templates of $Mg(OH)_2$ nanoflakes. The as-prepared CoNC materials present a porous and hierarchical framework with abundant interconnected large pores (**Figure 2**a and Figure S1 (Supporting Information)). The few-layered graphene flakes are dominantly with in-plane nanosized holes (Figure 2b). The pore size distribution further demonstrates abundant nanoscale pores ranged from several to tens of nanometers in CoNC material (Figure S2, Supporting Information). The hierarchical CoNC material with abundant micro-/mesopores in-plane and macrosized strutted spaces between sheets is beneficial for rapid diffusion of Li ions during the repeated plating/stripping process, which favors high-rate cycling performance. A metal-free counterpart prepared without cobalt nitrate addition (N-doped graphene matrix, denoted as NGM) possesses the similar features in pore structure (Figure S3a–c, Supporting Information). The specific surface areas of CoNC and NGM materials are 719.7 and 516.6 m^2 g^{-1}, while the total surface area of CoNC host (0.58 m^2) in the composite anode is approaching that of NGM host (0.57 m^2) (Figure S3, Supporting Information). Therefore, the influence of surface area on the following electrochemical performance between these two samples can be excluded.

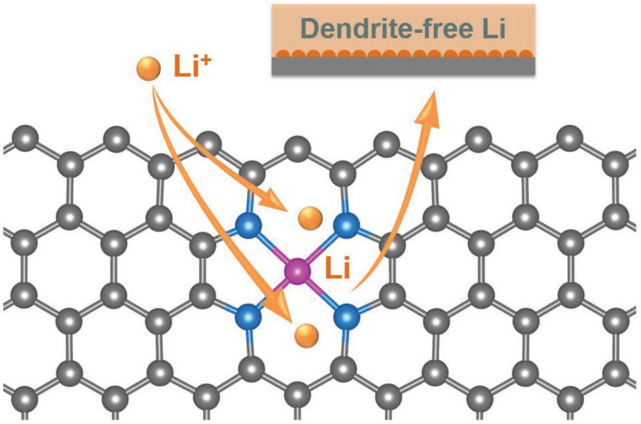

Figure 1. Schematic diagram of CoNC material and preferential Li nucleation sites. The carbon, nitrogen, and cobalt are marked with gray, blue, and deep pink, respectively.

No obvious bulk or aggregated cobalt-derived nanoparticles can be found in the high-resolution transmission electron microscopy (HRTEM) images (Figure 2b and Figure S1c,d (Supporting Information)), implying a well-dispersed feature of these Co sites. The energy dispersive spectroscopy (EDS) mapping of CoNC indicates a weak signal but a uniform distribution of Co as well as homogenous N element (Figure S4, Supporting Information). The content of cobalt in CoNC is 0.40 wt% determined by inductively coupled plasma optical emission spectrometer. High-angle annular dark field scanning transmission electron microscopy (HAADF-STEM) with spherical aberration electron beam was employed to probe the existence state of Co species. The heavy single Co atoms can be discerned in the carbon support because of a different *Z*-contrast between Co and C.[52] The images obtained by HAADF-STEM display highly dispersed isolated white dots (highlighted by yellow circles), which is attributed to isolated Co atoms (Figure 2c). A few very bright dots represent the overlap of two or more Co single atoms projected along the electron beam direction. When checking CoNC materials in randomly selected regions, single Co atoms were found to homogeneously distribute on carbon support (Figure S5, Supporting Information).

X-ray photoelectron spectroscopy (XPS) analysis reveals that the nitrogen content in CoNC materials is 1.77 at%, while no significant Co 2p peak can be detected due to its ultralow content (Figure S3e, Supporting Information). N 1s spectrum for CoNC reveals the coexistence of pyridinic (398.4 eV), pyrrolic (400.5 eV), graphitic (401.4 eV), oxidized (403.0 eV), and chemisorbed (405.2 eV) nitrogen species (Figure 2d). Compared with NGM (Figure S3f, Supporting Information), a new peak at 399.3 eV can be assigned to the N coordinated with Co, manifesting the presence of CoN_x species.[53,54] These results strongly indicate a high dispersion of single Co atoms in the porous CoNC layers with $Co—N_x—C$ configurations, which can potentially realize uniform deposition of Li metal.

The Li nucleation behavior is efficiently regulated by uniform and strong lithiophilicity of conductive hosts. First-principle calculations were performed to investigate the lithiophilicity of

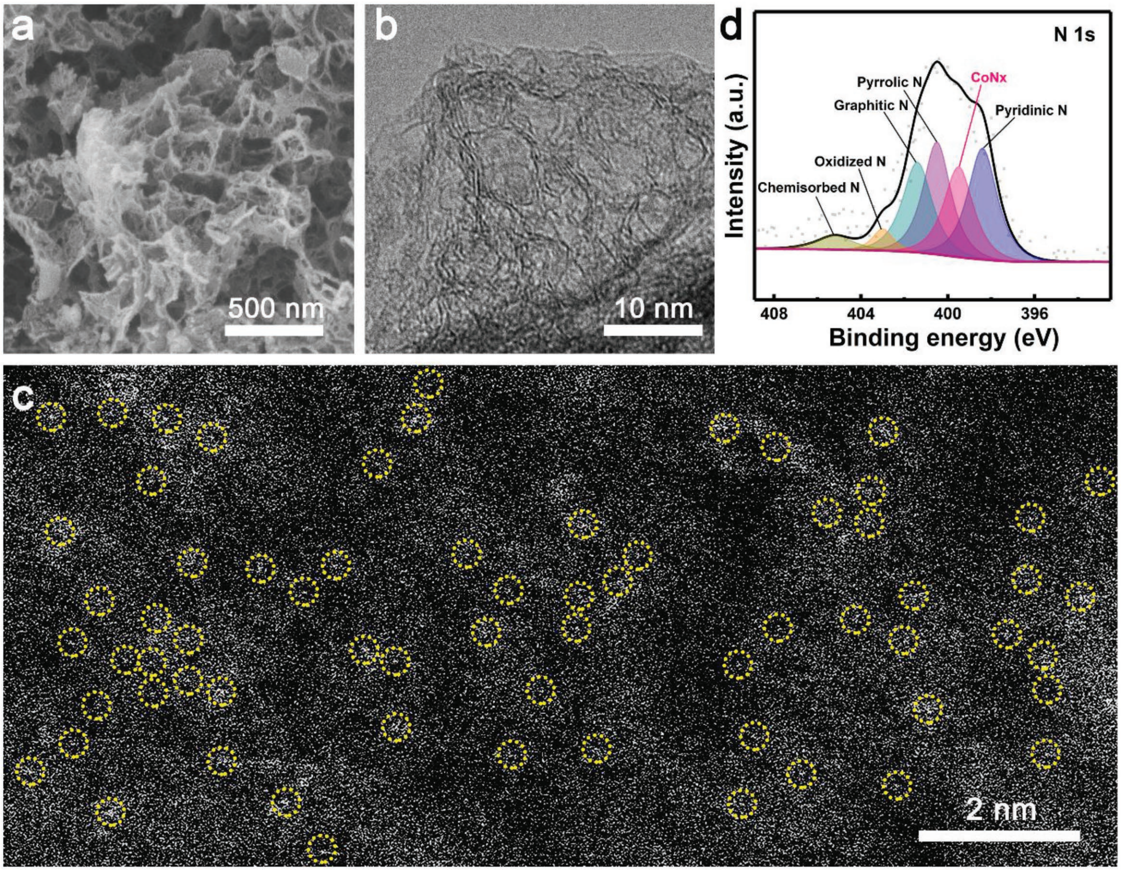

Figure 2. Characterizations of CoNC materials. a) SEM image, b) HRTEM image, and c) HAADF-STEM image of CoNC materials. d) XPS spectrum of N 1s for CoNC materials.

CoNC materials. Generally, Li can be absorbed on one top site (T) and three hollow sites (H1, H2, and H3) of CoNC, of which H1 site affords the largest binding energy (–1.58 eV) toward a Li atom (**Figure 3**a,b and Figure S6 (Supporting Information)). Herein, the graphitic N-doped graphene (NG) is used as the reference to avoid the edge effects by other N-doping (Figure S7, Supporting Information). As expected, all the binding energies induced by CoN_x sites in CoNC are much larger than that of N sites in NG (–0.86 eV). These results confirm the introducing of $Co{-}N_x{-}C$ structures into graphene can greatly enhance its lithiophilicity. Besides, the excellent lithiophilicity is achieved by the synergy between Co and N atoms. On one hand, the binding energy of H1 and H2 sites (Li interacts with N and Co simultaneously) is larger than that of H3 and T sites (Li interacts with N or Co). On the other hand, the differential charge density (Figure S8, Supporting Information) shows the electron gain between Li and N/Co atoms, indicating the Li atom bonds with N and Co in CoNC simultaneously. The synergy of N and Co interactions is responsible for the enhanced lithiophilicity of CoNC host.

The nucleation overpotential of different hosts was measured to evaluate the lithiophilicity and nucleation process on the electrode surface. A matrix with strong lithiophilicity favors Li nucleation with a reduced nucleation overpotential. The CoNC electrode exhibits the lowest nucleation overpotential at different current densities from 0.01 to 1.0 mA cm^{-2} compared with Cu and NGM electrodes (Figure 3c and Figure S9 (Supporting Information)). This is rationalized by the strong lithiophilicity provided by CoN_x moieties. Notably, doped N is the main nucleation sites for Li, and high content of doped N contributes to lower nucleation overpotential. Though the N content in CoNC (1.77 at%) is only one third of that in NGM (5.91 at%), its nucleation overpotential is actually 1–6 mV lower than that of NGM electrode at the same current density (Figure 3c). This result highlights the critical role of coordinated Co species in enhancing the lithiophilicity of carbon matrix, thus reducing the nucleation overpotential of CoNC host.

TEM images are employed to illustrate the Li nucleation behavior at CoNC host visually (Figure 3d). Dense black spots smaller than 10 nm in diameter are uniformly distributed on the surface of CoNC hosts (highlighted by white circles). These can be identified as the nucleation sites.[33] Li ions thereafter tend to absorb and grow up on these sites. Low-resolution TEM image demonstrates homogenously dispersed nucleation sites at a large scale (Figure S10, Supporting Information). The uniform nucleation sites induced by lower nucleation overpotential in CoNC materials are prerequisite for the uniform deposition of Li and finally achieving a dendrite-free morphology in Li metal anodes.

During the following Li deposition process, it can be observed that CoNC electrode displays a dendrite-free morphology with Li uniformly depositing on the surface of CoNC

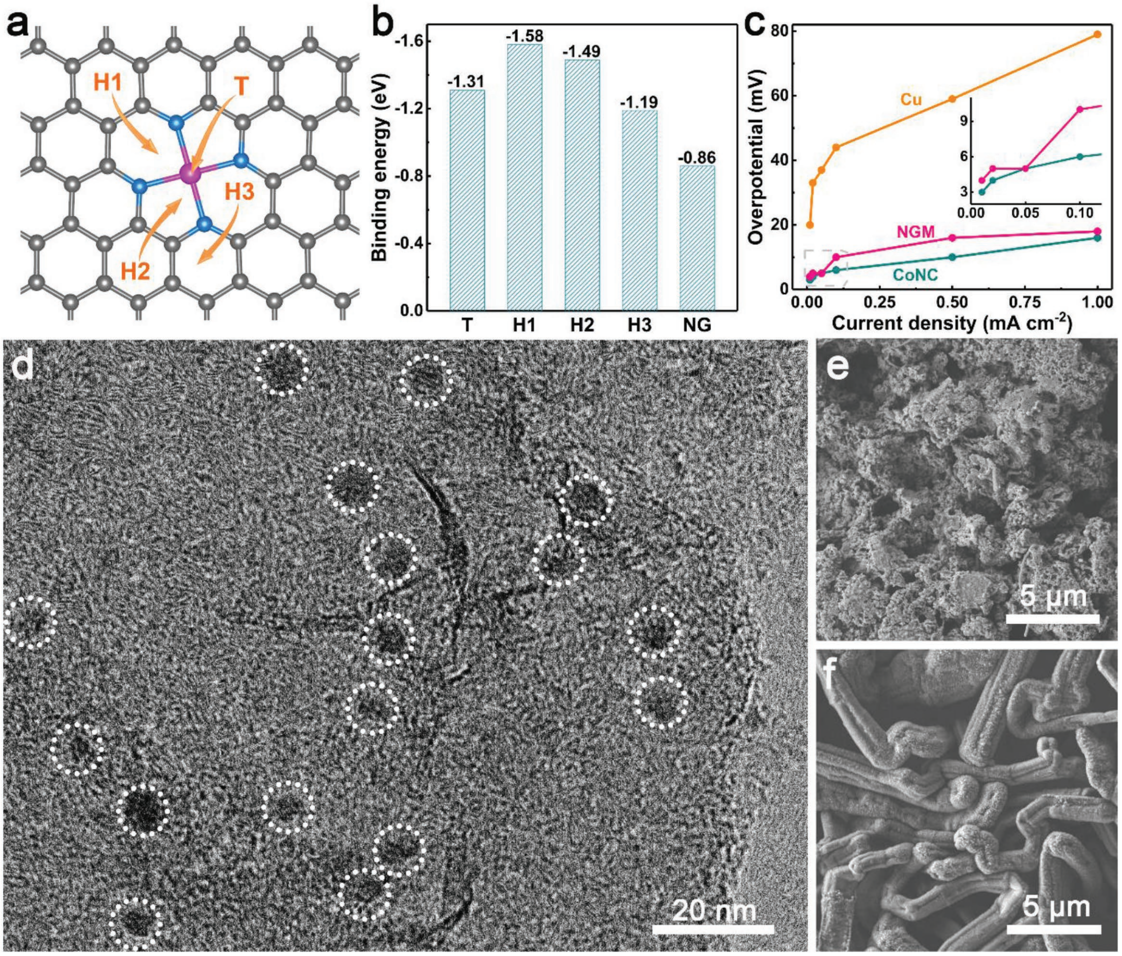

Figure 3. Nucleation and deposition of Li metal. a) Li adsorption sites on CoNC. The carbon, nitrogen, and cobalt are marked with gray, blue, and deep pink, respectively. b) The summary of binding energies between a Li atom and different adsorption sites on CoNC. NG is used as the reference. c) Li nucleation overpotentials on Cu, CoNC, and NGM electrodes at different current densities. d) TEM image of Li nucleation sites on CoNC at 0.1 mA cm^{-2} for 5 min. SEM images of e) CoNC and f) Cu electrodes after plating 2.0 mAh cm^{-2} of Li at 0.5 mA cm^{-2}.

nanoflakes at a low capacity of 0.5 mAh cm^{-2} (Figure S11b, Supporting Information). As the lithiation capacity increases to 1.0 mAh cm^{-2}, the interspaces between the graphene flakes are filled with more Li deposits (Figure S11a–c, Supporting Information), while the deposition morphology remains almost unchanged without any dendrite formation. Further increasing the capacity to 2.0 mAh cm^{-2}, most of the interspaces are full of Li deposits (Figure 3e), and Li starts to plate on the surface of CoNC electrode (Figure S11d, Supporting Information). Remarkably, a thin layer of Li compactly covers on the whole electrode uniformly, rather than forming uncontrollable Li dendrites. The scanning electron microscopy (SEM) images of CoNC anode with different capacities clearly depict the Li depositing process (Figure S12, Supporting Information). The CoNC flakes are wrapped by densely but uniformly distributed particles assigned to Li species with dozens of nanometers at a low capacity of 0.5 mAh cm^{-2} (Figure S12b, Supporting Information). This is a direct evidence that Li tends to deposit and grow up on the initial nucleation sites (Figure 3d). As the lithiation capacity increases, the particles keep growing and finally coalesce with each other to form a smooth layer of Li deposits with visible protuberances covered the surface of flakes and their gaps (Figure S12c,d, Supporting Information). The uniform deposition behavior in CoNC host can be ascribed to the homogenously distributed CoN$_x$ species with strong lithiophilicity.

By contrast, Li plates randomly with large amounts of visible Li dendrites even at an ultralow capacity of 0.1 mAh cm^{-2} on the surface of Cu electrode without any lithiophilic site (Figure S11e, Supporting Information). Extended plating time accompanies with Li dendrites growing thicker and longer. The filaments have a diameter of around several micrometers and a length of dozens of micrometers at a capacity of 2.0 mAh cm^{-2} (Figure 3f and Figure S11e–h (Supporting Information)). These large dendrites not only induce huge safety risk, but also cause poor efficiency of LMBs. The above results underscore the critical role of initial nucleation state in determining the following plating process and the final Li deposition morphology.

The morphologies of CoNC and Cu anodes after galvanostatic stripping/plating for 200 cycles at large current densities (2.0 and 5.0 mA cm^{-2}) were further investigated. For Cu electrode, the anode surface has large amounts of irregular

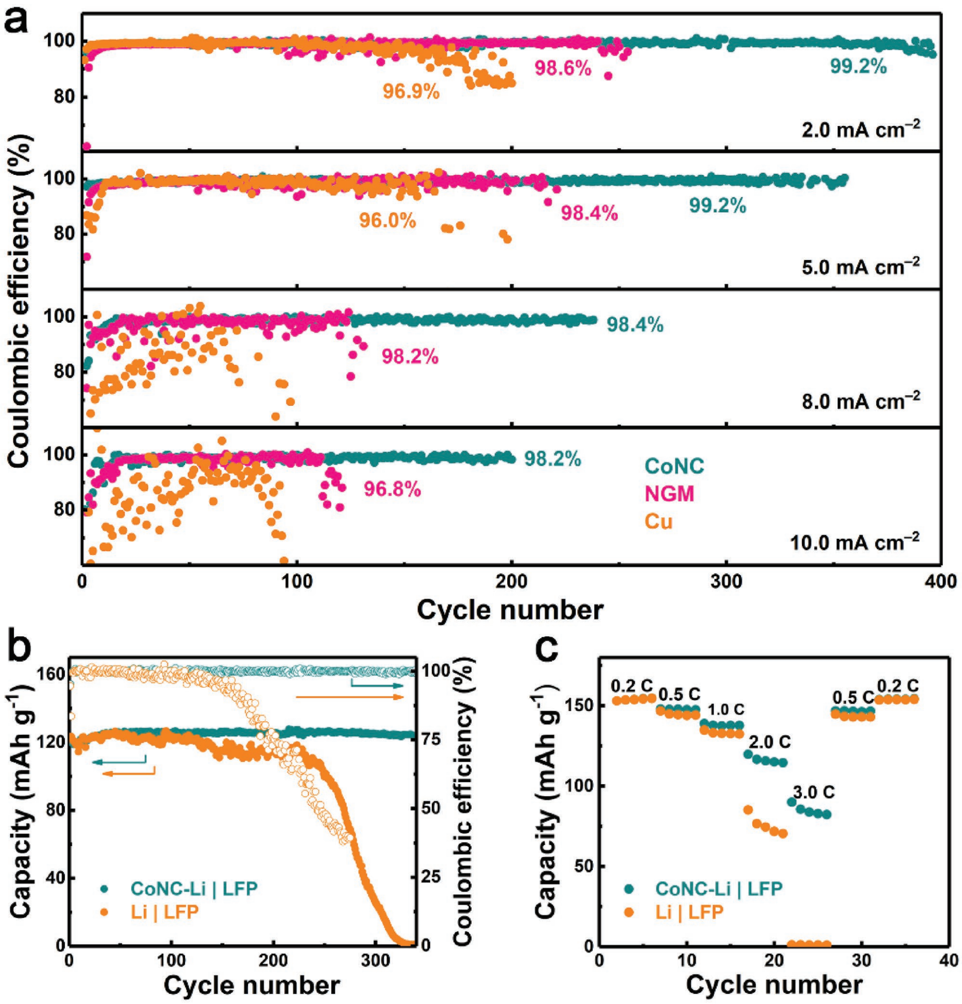

Figure 4. Long-term electrochemical cycling performance. a) CE of CoNC, NGM, and Cu electrodes at a fixed capacity of 2.0 mAh cm^{-2}. b) Long-term cycling at 1.0 C (1.0 C = 170 mA g^{-1} = 1.1 mA cm^{-2}) and c) rate capability performance of CoNC–Li|LFP and Li|LFP full cells.

dendrites after plating 2.0 mAh cm^{-2} Li at 2.0 mA cm^{-2} (Figure S13a, Supporting Information). This situation becomes even worse with increasing current density to 5.0 mA cm^{-2}, and the filaments interconnect with each other forming loose dendrite structures with a lot of voids (Figure S13b, Supporting Information). After stripping Li from Cu anode, these loose structures are prone to detaching from the electrode surface, generating dead Li wrapped by unstable SEI (Figure S14a,b, Supporting Information). While in the CoNC electrode, Li plates on the conductive CoNC host smoothly without any dendrite growth after 200 cycles at 2.0 and 5.0 mA cm^{-2} (Figure S13c,d, Supporting Information), resulting from the uniform Li nucleation and deposition behavior on the matrix at the initial stage. In the following stripping process, Li strips from the surface of CoNC flakes and their gaps, leaving conductive CoNC host surrounded by SEI (Figure S14c,d, Supporting Information). CoNC host affords the space to accommodate the huge volume change during the repeated plating/stripping process, avoiding the formation of dead Li and favoring the generation of stable SEI. This is of great significance for improving the long cycling performance of Li metal batteries.

The uniform Li nucleation and deposition morphology on CoNC matrix can potentially improve the reversibility of Li metal anode during repeated plating/stripping. The CE of Li deposition on Cu foil, CoNC, and NGM electrodes were probed with an areal capacity of 2.0 mAh cm^{-2} (**Figure 4**a). Herein, the CE is defined as the ratio of the Li amount stripped away from the working electrode to that of Li plated in each cycle. A stable and high CE of 99.2% for nearly 400 cycles is achieved at 2.0 mA cm^{-2} and 350 cycles at 5.0 mA cm^{-2} on CoNC host. This indicates a very high degree of reversible Li in CoNC electrode, as confirmed by the Li plating/stripping morphology at 200 cycles in Figures S13 and S14 (Supporting Information). By contrast, NGM electrode delivers small CE of 98.6% and 98.4% at 2.0 and 5.0 mA cm^{-2} for ~200 cycles, respectively. Cu electrode exhibits an inferior electrochemical cycling performance with fluctuant CE and service life less than 200 cycles. Furthermore, the uniform Li plating/stripping in CoNC host still promises high and stable CE of 98.4% and 98.2% at 8.0 and 10.0 mA cm^{-2}, respectively, with a long lifespan over 200 cycles. However, the CE of NGM and Cu electrodes fluctuates with sharply declining service time at such high currents.

This is induced by the rapid dendrite formation and unstable SEI layer. The higher and more stable CE with longer lifespan in CoNC electrode validates the superiority of strong lithiophilicity of host in improving the utilization and reversibility of Li deposition.

The concentrated electrolyte contributes to forming a highly compact and stable SEI at high-rate cycling of Li metal anodes. This can be verified by the inferior cycling stability and CE performance using routine carbonate electrolyte (1.0 M $LiPF_6$ in ethylene carbonate/diethyl carbonate (EC/DEC)) (Figure S15, Supporting Information), in which Li metal is easily corroded. Although the service life of CoNC electrodes is much longer than that of Cu electrodes, their CE are below 85.0%, even at a current density of 2.0 mA cm^{-2} and a capacity of 1.0 mAh cm^{-2}. Therefore, the concentrated electrolyte constructs a stable and compact SEI on anode surface at an early stage of cycling. The lithiophilic CoNC host maintains the stability of SEI by accommodating Li deposits and relieving volume change during the long cycling. The synergy of concentrated electrolyte and CoNC host contributes to the ultrahigh CE at high rates and excellent cycling performance.

Li metal electrode reversibility strongly relates with the transfer resistance of Li ions and electrons, and an inferior CE always accompanies with increased polarization in voltage profiles (Figure S16, Supporting Information). In Cu anode, a voltage hysteresis of ≈80 mV before 100th cycle increases to ≈90 mV at 200th cycle (Figure S16a, Supporting Information). Both CoNC and NGM electrodes exhibit flat voltage plateaus with a proximate voltage hysteresis of 70 mV during the initial 100 cycles. The stable voltage plateaus can be retained without increasing in hysteresis for 400 cycles in CoNC anode (Figure S16b, Supporting Information), while an obviously increased hysteresis to 100 mV in NGM anode is observed after 250 cycles (Figure S16c, Supporting Information). The low hysteresis and superior cycling stability of CoNC electrode suggest a stable SEI film, which is attributed to the uniform Li deposits. Notably, CoNC electrode delivers better reversibility and lower nucleation overpotential during the whole cycles than NGM electrode, further highlighting the advantages of strong lithiophilicity of CoN_x species. The dynamic nature of Li ion and electron transfer was also performed by electrochemical impedance spectroscopy (EIS) (Figure S17, Supporting Information). A much lower SEI resistance (semicircle at mid-frequency) and charge transfer resistance (straight lines at low-frequency) of CoNC host than Cu confirms a stable SEI with high ionic conductivity and hence a uniform Li deposition in the lithiophilic CoNC host. Therefore, CoNC electrode exhibits impressive capability in both Li dendrite inhibition and electrochemical performance. All these improvements mainly benefit from the effective regulation on Li nucleation and the following growth process contributed by the superb lithiophilicity.

CoNC–Li|LFP full cell was assembled with CoNC–Li composite anode and LFP cathode to investigate the potential in practical applications of the CoNC matrix. The composite anode was fabricated through pressing CoNC matrix onto the ultrathin Li foil (50 µm thick, ≈10 mAh cm^{-2}) and Li metal deposits into the host gradually during cycling. Routine binary carbonate electrolyte (1.0 M $LiPF_6$ in EC/DEC) was employed herein. 5 µL of concentrated electrolyte, 3 M lithium bis(fluorosulfonyl)imide (LiFSI) in 1,2-dimethoxyethane (DME), was used to prewet the CoNC matrix and Li foil to construct a compact and stable SEI on the anode surface upon precycling process, preventing corrosion of Li metal anode from carbonate electrolyte. CoNC–Li|LFP cell displays a much better cycling performance and lower polarization than routine Li (50 µm thick)|LFP cells at 1.0 C (1.0 C = 170 mA g^{-1}) (Figure 4b and Figure S18 (Supporting Information)). The cell with CoNC–Li composite anode achieves a capacity retention of 98.4% with a CE of 99.9% after 340 cycles, while the capacity retention in routine Li|LFP cell drops to below 90.0% after 150 cycles with an average CE of 98.4%. The rapid failure of Li|LFP full cells is mainly caused by the depletion of limited Li source (50 µm thick, 200–500 µm for commercial Li foils) in anode side, as indicated by the accelerated decay of CE after 150 cycles. By contrast, the CE in CoNC–Li|LFP cell keeps at 99.9% even after 340 cycles, suggesting that lithiophilic CoNC host can maintain the stable SEI and achieve a high utilization of Li metal during the long cycling by accommodating the Li deposits and alleviating the volume change. CoNC–Li|LFP cell also delivers a better rate capability (Figure 4c). Especially at high rates of 2.0 and 3.0 C, a capacity of ≈115 and ≈85 mAh g^{-1} can be obtained, respectively, which is much higher than that of routine Li|LFP cell (merely ≈75 and ≈1 mAh g^{-1}, respectively) (Figure S19, Supporting Information). These results convincingly demonstrate a stable and uniform deposition behavior in CoNC host, which can efficiently increase the reversibility of working Li metal anodes.

In conclusion, CoNC materials with atomically dispersed CoN_x species are proved to be critically effective in regulating Li nucleation and deposition behavior. Impressively, CoNC anode exhibits a CE of 99.2% for 400 and 300 cycles at 2.0 and 5.0 mA cm^{-2}, and >98% at 8.0 and 10.0 mA cm^{-2}. The full cell with LFP cathode also exhibits better cycling performance, higher rate capability, and smaller polarization. The superior electrochemical performance of CoNC anode originates from the stronger lithiophilicity provided by the highly dispersed CoN_x species, which enables uniform Li nucleation and deposition without any dendrite formation. The CoNC material can serve as an excellent host for Li metal anode with superior dendrite suppression and electrochemical performance. This work innovates the chemistry of energy materials that can effectively regulate the interactions between Li ions and hosts. This sheds fresh lights on the safe and efficient operation of LMBs and other metallic batteries.

Supporting Information

Supporting Information is available from the Wiley Online Library or from the author.

Acknowledgements

This work was supported by the National Key Research and Development Program (Grant Nos. 2016YFA0202500, 2016YFA0200102, and 2015CB932500), the National Natural Scientific Foundation of China (Grant Nos. 21676160, 21825501, 21808121, and 21805161), and the China Postdoctoral Science Foundation (Grant Nos. 2017M620773, 2018M631480, and BX201700125). The authors acknowledge the support from the Tsinghua National Laboratory for Information Science and Technology for theoretical simulations.

Conflict of Interest

The authors declare no conflict of interest.

Keywords

Co/N/C host, lithiophilic chemistry, lithium metal batteries, lithium metal dendrites

Received: September 11, 2018
Revised: October 30, 2018

---

[1] J. B. Goodenough, K.-S. Park, *J. Am. Chem. Soc.* **2013**, *135*, 1167.
[2] K. N. Wood, M. Noked, N. P. Dasgupta, *ACS Energy Lett.* **2017**, *2*, 664.
[3] J. M. Tarascon, M. Armand, *Nature* **2001**, *414*, 359.
[4] S. Jiao, J. Zheng, Q. Li, X. Li, M. H. Engelhard, R. Cao, J.-G. Zhang, W. Xu, *Joule* **2018**, *2*, 110.
[5] J. Wang, F. Lin, H. Jia, J. Yang, C. W. Monroe, Y. NuLi, *Angew. Chem., Int. Ed.* **2014**, *53*, 10099.
[6] Z. Gao, H. Sun, L. Fu, F. Ye, Y. Zhang, W. Luo, Y. Huang, *Adv. Mater.* **2018**, *30*, 1705702.
[7] P. G. Bruce, S. A. Freunberger, L. J. Hardwick, J.-M. Tarascon, *Nat. Mater.* **2012**, *11*, 19.
[8] D. Lin, Y. Liu, Y. Cui, *Nat. Nanotechnol.* **2017**, *12*, 194.
[9] J. Lang, L. Qi, Y. Luo, H. Wu, *Energy Storage Mater.* **2017**, *7*, 115.
[10] B. Zhou, L. Guo, Y. Zhang, J. Wang, L. Ma, W.-H. Zhang, Z. Fu, Z. Peng, *Adv. Mater.* **2017**, *29*, 1701568.
[11] Y. Lu, S. Gu, X. Hong, K. Rui, X. Huang, J. Jin, C. Chen, J. Yang, Z. Wen, *Energy Storage Mater.* **2018**, *11*, 16.
[12] L. Li, S. Li, Y. Lu, *Chem. Commun.* **2018**, *54*, 6648.
[13] W. Liu, Y. Mi, Z. Weng, Y. Zhong, Z. Wu, H. Wang, *Chem. Sci.* **2017**, *8*, 4285.
[14] S. Wang, H. Xu, W. Li, A. Dolocan, A. Manthiram, *J. Am. Chem. Soc.* **2018**, *140*, 250.
[15] L. Xu, S. Tang, Y. Cheng, K. Wang, J. Liang, C. Liu, Y.-C. Cao, F. Wei, L. Mai, *Joule* **2018**, *2*, 1991.
[16] G. Li, Q. Huang, X. He, Y. Gao, D. Wang, S. H. Kim, D. Wang, *ACS Nano* **2018**, *12*, 1500.
[17] F. Ding, W. Xu, G. L. Graff, J. Zhang, M. L. Sushko, X. Chen, Y. Shao, M. H. Engelhard, Z. Nie, J. Xiao, X. Liu, P. V. Sushko, J. Liu, J.-G. Zhang, *J. Am. Chem. Soc.* **2013**, *135*, 4450.
[18] H. Ota, K. Shima, M. Ue, J.-i. Yamaki, *Electrochim. Acta* **2004**, *49*, 565.
[19] S. Choudhury, L. A. Archer, *Adv. Electron. Mater.* **2016**, *2*, 1500246.
[20] J. Zheng, J. A. Lochala, A. Kwok, Z. D. Deng, J. Xiao, *Adv. Sci.* **2017**, *4*, 1700032.
[21] C.-Z. Zhao, X.-Q. Zhang, X.-B. Cheng, R. Zhang, R. Xu, P.-Y. Chen, H.-J. Peng, J.-Q. Huang, Q. Zhang, *Proc. Natl. Acad. Sci. USA* **2017**, *114*, 11069.
[22] D. Zhou, R. Liu, Y.-B. He, F. Li, M. Liu, B. Li, Q.-H. Yang, Q. Cai, F. Kang, *Adv. Energy Mater.* **2016**, *6*, 1502214.
[23] W. Luo, Y. Gong, Y. Zhu, K. K. Fu, J. Dai, S. D. Lacey, C. Wang, B. Liu, X. Han, Y. Mo, E. D. Wachsman, L. Hu, *J. Am. Chem. Soc.* **2016**, *138*, 12258.
[24] N. Chen, Y. Dai, Y. Xing, L. Wang, C. Guo, R. Chen, S. Guo, F. Wu, *Energy Environ. Sci.* **2017**, *10*, 1660.
[25] J. Zhang, J. Yang, T. Dong, M. Zhang, J. Chai, S. Dong, T. Wu, X. Zhou, G. Cui, *Small* **2018**, *14*, 1800821.
[26] S. Ali, C. Tan, M. Waqas, W. Lv, Z. Wei, S. Wu, B. Boateng, J. Liu, J. Ahmed, J. Xiong, J. B. Goodenough, W. He, *Adv. Mater. Interfaces* **2018**, *5*, 1701147.
[27] X. Cheng, J. Pan, Y. Zhao, M. Liao, H. Peng, *Adv. Energy Mater.* **2018**, *8*, 1702184.
[28] Q.-C. Liu, J.-J. Xu, S. Yuan, Z.-W. Chang, D. Xu, Y.-B. Yin, L. Li, H.-X. Zhong, Y.-S. Jiang, J.-M. Yan, X.-B. Zhang, *Adv. Mater.* **2015**, *27*, 5241.
[29] R. Xu, X.-Q. Zhang, X.-B. Cheng, H.-J. Peng, C.-Z. Zhao, C. Yan, J.-Q. Huang, *Adv. Funct. Mater.* **2018**, *28*, 1705838.
[30] Q. Pang, X. Liang, A. Shyamsunder, L. F. Nazar, *Joule* **2017**, *1*, 871.
[31] Y. Zhao, X. Yang, Q. Sun, X. Gao, X. Lin, C. Wang, F. Zhao, Y. Sun, K. R. Adair, R. Li, M. Cai, X. Sun, *Energy Storage Mater.* **2018**, *15*, 415.
[32] N.-W. Li, Y. Shi, Y.-X. Yin, X.-X. Zeng, J.-Y. Li, C.-J. Li, L.-J. Wan, R. Wen, Y.-G. Guo, *Angew. Chem., Int. Ed.* **2018**, *57*, 1505.
[33] L. Fan, L. Zhuang Houlong, W. Zhang, Y. Fu, Z. Liao, Y. Lu, *Adv. Energy Mater.* **2018**, *8*, 1703360.
[34] D. Lin, Y. Liu, Z. Liang, H.-W. Lee, J. Sun, H. Wang, K. Yan, J. Xie, Y. Cui, *Nat. Nanotechnol.* **2016**, *11*, 626.
[35] T.-T. Zuo, X.-W. Wu, C.-P. Yang, Y.-X. Yin, H. Ye, N.-W. Li, Y.-G. Guo, *Adv. Mater.* **2017**, *29*, 1700389.
[36] L.-L. Lu, J. Ge, J.-N. Yang, S.-M. Chen, H.-B. Yao, F. Zhou, S.-H. Yu, *Nano Lett.* **2016**, *16*, 4431.
[37] T. Wang, R. Villegas Salvatierra, A. S. Jalilov, J. Tian, J. M. Tour, *ACS Nano* **2017**, *11*, 10761.
[38] C. Zhang, S. Liu, G. Li, C. Zhang, X. Liu, J. Luo, *Adv. Mater.* **2018**, *30*, 1801328.
[39] L.-L. Lu, Y. Zhang, Z. Pan, H.-B. Yao, F. Zhou, S.-H. Yu, *Energy Storage Mater.* **2017**, *9*, 31.
[40] H. Zhao, D. Lei, Y.-B. He, Y. Yuan, Q. Yun, B. Ni, W. Lv, B. Li, Q.-H. Yang, F. Kang, J. Lu, *Adv. Energy Mater.* **2018**, *8*, 1800266.
[41] R. Zhang, X. Chen, X. Shen, X.-Q. Zhang, X.-R. Chen, X.-B. Cheng, C. Yan, C.-Z. Zhao, Q. Zhang, *Joule* **2018**, *2*, 764.
[42] L. Wang, X. Zhu, Y. Guan, J. Zhang, F. Ai, W. Zhang, Y. Xiang, S. Vijayan, G. Li, Y. Huang, G. Cao, Y. Yang, H. Zhang, *Energy Storage Mater.* **2018**, *11*, 191.
[43] Q. Song, H. Yan, K. Liu, K. Xie, W. Li, W. Gai, G. Chen, H. Li, C. Shen, Q. Fu, S. Zhang, L. Zhang, B. Wei, *Adv. Energy Mater.* **2018**, *8*, 1800564.
[44] M. Zhu, B. Li, S. Li, Z. Du, Y. Gong, S. Yang, *Adv. Energy Mater.* **2018**, *8*, 1703505.
[45] Z. Jiang, T. Liu, L. Yan, J. Liu, F. Dong, M. Ling, C. Liang, Z. Lin, *Energy Storage Mater.* **2018**, *11*, 267.
[46] C. Jin, O. Sheng, Y. Lu, J. Luo, H. Yuan, W. Zhang, H. Huang, Y. Gan, Y. Xia, C. Liang, J. Zhang, X. Tao, *Nano Energy* **2018**, *45*, 203.
[47] R. Zhang, X. R. Chen, X. Chen, X. B. Cheng, X. Q. Zhang, C. Yan, Q. Zhang, *Angew. Chem., Int. Ed.* **2017**, *56*, 7764.
[48] G. Hou, X. Ren, X. Ma, L. Zhang, W. Zhai, Q. Ai, X. Xu, L. Zhang, P. Si, J. Feng, F. Ding, L. Ci, *J. Power Sources* **2018**, *386*, 77.
[49] G. Wan, P. Yu, H. Chen, J. Wen, C.-j. Sun, H. Zhou, N. Zhang, Q. Li, W. Zhao, B. Xie, T. Li, J. Shi, *Small* **2018**, *14*, 1704319.
[50] D. Deng, X. Chen, L. Yu, X. Wu, Q. Liu, Y. Liu, H. Yang, H. Tian, Y. Hu, P. Du, R. Si, J. Wang, X. Cui, H. Li, J. Xiao, T. Xu, J. Deng, F. Yang, P. N. Duchesne, P. Zhang, J. Zhou, L. Sun, J. Li, X. Pan, X. Bao, *Sci. Adv.* **2015**, *1*, e1500462.
[51] S. Kattel, G. Wang, *J. Mater. Chem. A* **2013**, *1*, 10790.
[52] Y. Han, Y.-G. Wang, W. Chen, R. Xu, L. Zheng, J. Zhang, J. Luo, R.-A. Shen, Y. Zhu, W.-C. Cheong, C. Chen, Q. Peng, D. Wang, Y. Li, *J. Am. Chem. Soc.* **2017**, *139*, 17269.
[53] C. Tang, B. Wang, H.-F. Wang, Q. Zhang, *Adv. Mater.* **2017**, *29*, 1703185.
[54] F. Pan, H. Zhang, K. Liu, D. Cullen, K. More, M. Wang, Z. Feng, G. Wang, G. Wu, Y. Li, *ACS Catal.* **2018**, *8*, 3116.